We are IntechOpen, the world's leading publisher of Open Access books Built by scientists, for scientists

6,900
Open access books available

185,000
International authors and editors

200M
Downloads

Our authors are among the

154
Countries delivered to

TOP 1%
most cited scientists

12.2%
Contributors from top 500 universities



WEB OF SCIENCE™

Selection of our books indexed in the Book Citation Index in Web of Science™ Core Collection (BKCI)

Interested in publishing with us?
Contact book.department@intechopen.com

Numbers displayed above are based on latest data collected.
For more information visit www.intechopen.com



14

Morphology and Dispersion of Pristine and Modified Carbon Nanofibers in Water

Jian Zhao
Qingdao University of Science and Technology, Qingdao, China, and Department of Chemical and Materials Engineering, University of Cincinnati, Cincinnati, OH, USA

1. Introduction

Carbon nanofibers have been of great interest due to their extraordinary mechanical and electronic properties. Carbon nanofibers (CNF) are different from carbon nanotubes in that they have many more walls of crystalline carbon and usually have more structural defects than carbon nanotubes. The cost of preparing carbon nanofibers is significantly less than carbon nanotubes due to the synthesis techniques used, defects and the remaining amorphous carbon.

Carbon nanofibers are suitable for a range of applications such as reinforcing fillers, field emitters and nanoelectronic devices etc. (Dresselhaus, Dresselhaus et al. 2001; Safadi, Andrews et al. 2002; Gong, Li et al. 2005; Li, Zhao et al. 2005) Unfortunately, the advantages of carbon nanofibers have not been realized because of the difficulty of obtaining fully dispersed nanofibers. Although hundreds of papers have been published describing enhanced dispersion of carbon nanofibers by surface modification, plasma treatment and functionalization of the sidewalls and fiber tips, quantitative measurement of the degree of dispersion remains challenging and the nature of the dispersed entities remains unknown.

Scattering methods is an ideal tool to provide structural information about nanofiber morphology. In this chapter, we review several approaches that are used to assist dispersion, including surface modification, PEG-functionalization and plasma treatment Small angle light scattering is utilized as a primary tool to assess the morphology of the carbon nanofibers and quantify dispersion of the carbon nanofibers treated through these approaches. A simplified tube or fiber model is introduced to assist in further understanding the morphology. The chapter is divided into three sections.

The first section focuses on dispersion of untreated and acid-treated carbon nanofibers suspended in water. Analysis of Light scattering data provides the first insights into the mechanism by which surface treatment promotes dispersion. Both acid-treated and untreated nanofibers exhibit hierarchical morphology consisting of small-scale aggregates (bundles) that agglomerate to form fractal clusters that eventually precipitate. Although the morphology of the aggregates and agglomerates is nearly independent of surface treatment, their time evolution is quite different. Acid oxidation has little effect on bundle morphology. Rather acid treatment slows agglomeration of the bundles. The second section discusses the morphology and dispersion of solubilized carbon nanofibers. Light scattering data indicate that PEG-functionalized nanofibers are dispersed at small rod-like bundle (side-by-side

Source: Nanofibers, Book edited by: Ashok Kumar,
ISBN 978-953-7619-86-2, pp. 438, February 2010, INTECH, Croatia, downloaded from SCIYO.COM

aggregate) level. PEG-functionalization of the carbon fibers leads to solubilization not by disrupting small-scale size-by-side bundles, but by inhibiting formation of the large-scale agglomerates. The third section focuses on dispersion of plasma-treated carbon nanofibers. Comparison of untreated and plasma-treated nanofibers shows that plasma treatment facilitates dispersion of nanofibers. The chapter will conclude with a summary.

1.1 Thermodynamics of nanophase carbon

In this section, the origin of the dispersion problem, mainly with respect to thermodynamics is explored. Several factors make the dispersion of nanophase carbon particularly troublesome. These factors are dominated by strong attraction between carbon species of both enthalpic and entropic origin. In addition, the low dimensionality of carbon nanotubes leads to an enhancement of these attractive forces.

The origin of the attractive forces between graphitic structures is well known. Due to the extended pi electron system, these systems are highly polarizable, and thus subject to large attractive van der Waals forces. These forces are responsible for the secondary bonding that holds graphitic layers together. In the case of carbon nanofibers, these forces lead to so called "bundles," extended structures formed by side-by-side aggregation of the nanofibers.

When suspended in a polymer, an attractive force between filler particles also arises due to pure entropic factors. (Bechinger, Rudhardt et al. 1999) Polymer chains in the corona region of the colloidal filler suffer an entropic penalty since roughly half of their configurations are precluded. Therefore there is a depletion of polymer in the corona. This depletion results in an osmotic pressure forcing the filler particles together. This effective attraction is intrinsic to colloids dispersed in polymers.

Finally, the linear structure of carbon nanotubes leads to a cooperative effect that enhances the forces described above. Whereas spherical particles touch at a point, rods interact along a line. As a result the above forces are augmented by filler geometry.

1.2 Structure and small-angle scattering:

Small-angle scattering is a powerful technique for characterization of fractal objects. Small angle scattering (SAS) is the collective name given to the techniques of small angle neutron (SANS), x-ray (SAXS) and light (SALS, or just LS) scattering. Fractal objects are geometrically self-similar under a transformation of scale. (Schaefer 1988) This self-similarity is implicit in the power-law functions. In a scattering experiment, however, self-similarity is manifest in a power-law relationship between intensity I and wave vector q.

$$I(q) \propto q^{-P} \tag{1}$$

In scattering experiments, the scattered intensity I(q), which is proportional to the scattering cross section per unit volume $d\Sigma/Vd\Omega$, is measured as a function of scattering angle θ. This angle is related to the wave vector, q.

$$q = 4n\pi/\lambda \sin(\theta/2) = 2\pi/d \tag{2}$$

where λ is the wavelength of the incident beam in the media, θ is the scattering angle, and d is the length scale probed in the experiment.

The scattered intensity, I(q), then is expressed as:

$$I(q) \propto NP^2(q)S(q) \tag{3}$$

where N is the number density of individual scatterers, P(q) is a form factor related to the shape and scattering crosssection of the scatterers and S(q) is the structure factor related to correlations between the scatterers.

In the scattering experiment, a beam of electromagnetic radiation strikes a sample. The radiation is elastically scattered by the sample. A detector records the scattered beam. The resulting scattering pattern can be analyzed to provide information about the size and shape etc. of nanoparticles. Scattering techniques effectively probe an object on different length scales as determined by q^{-1}. (Schaefer, Bunker et al. 1989)

In our study, we use small angle light scattering as a primary tool to investigate dispersion of nanofibers. The dispersion efficiency was determined using a low-angle light scattering photometer–a Micromeritics Saturn Digitizer (www.micromeritics.com). Light scattering data are reported in reciprocal space (intensity vs. wave vector, q). Data in this form are directly available. Light scattering covers the regime 10^{-6} Å^{-1} < q < 10^{-3} Å^{-1}. The q-range corresponds to length-scales (~q^{-1}) from 100 μm at low q to 1000 Å at high q. A scattering curve can be fitted over two-level regimes by a unified function related to the aggregated bundles and agglomerate structure respectively.

2. Acid-treated and As-received nanofibers

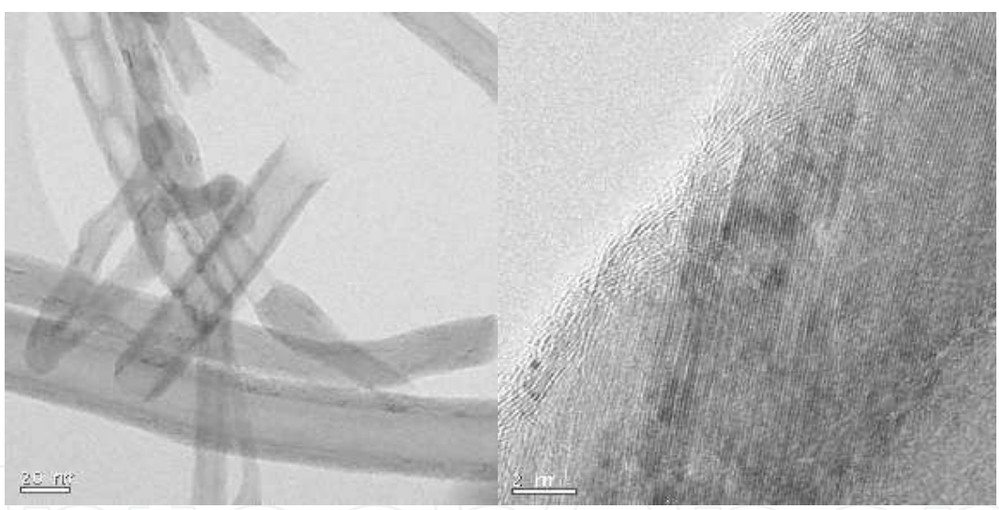


Fig. 1. TEMs of unmodified carbon nanofibers PR19HT. Graphitic layers are visible at both magnifications. The low-resolution image shows a variety of tube shapes and morphologies including concentric cylinders and stacked cones. No metallic catalyst was observed. The bars are 20 nm and 2 nm.

Applied Sciences, Inc. (ASI) made all the nanofiber samples used in this research using full scale chemical vapor deposition (CVD). A 3:1 concentrated H2SO4:HNO3 mixture is commonly used for surface modification. (Chen, Hamon et al. 1998; Chen, Rao et al. 2001) After such acid treatment, nanofibers form relatively stable colloidal solutions in water. Dispersions have been characterized by atomic force microscopy (AFM), UV/visible-NIR spectra etc. (Shaffer, Fan et al. 1998; Ausman, Piner et al. 2000) The evolution of the dispersed state under quiescent conditions following sonication, however, remains unknown. Here, we use light scattering to quantify the state dispersion of as-received and acid-treated carbon nanofibers as a function of time. To understand the state of aggregation

of the nanofibers, the size distribution from the light scattering data is determined using the maximum entropy (ME) method. (Potton, Daniell et al. 1988; Morrison, Corcoran et al. 1992; Boukari, Long et al. 2000) We used the Irena code (http://www.uni.aps.anl.gov/~ilavsky/irena.html) developed by Ilavsky and Jemian to obtain the maximum-entropy solution. (Jemian, Weertman et al. 1991; Ilavsky 2004)

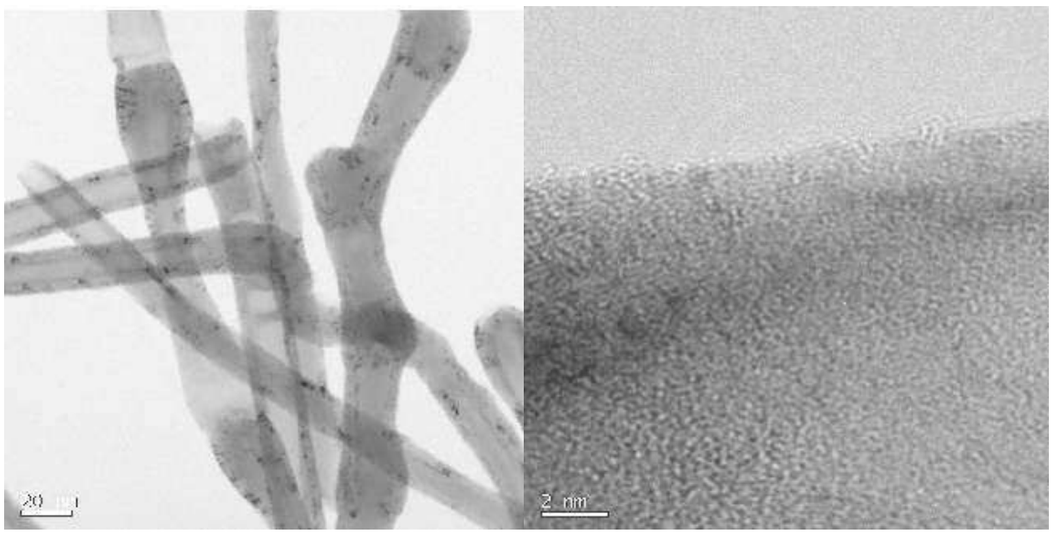


Fig. 2. TEMs of acid-treated nanofibers PR19LHT: More defects on the walls are evident and breakage of graphite layers. The bars are 20 nm and 2 nm.

2.1 Transmission Electron Microscopy (TEM)

The raw Pyrograf®-III PR19HT powder consists of loosely aggregated nanofibers. Some nanofibers are curved with open ends. A representative HRTEM image of the original Pyrograf®-III PR19HT (Figure 1) shows the graphite structure with the interlayer spacing d = 0.34 nm. No iron catalyst particles are found by TEM. Defects on the walls of nanofibers are occasionally observed in pristine nanofibers.

	Time	5min	1 hr	2 hr	5 hr	8 hr	24 hr	32hr	44hr
Low q	Rg (μm)	4.8	4.6	4.5	4.3	3.5	8.4	11.9	14.4
	P	1.04	1.07	1.09	1.01	1.00	1.29	1.45	1.78
	G	9.5	8.7	8.5	7.2	4.6	14.0	30.5	69.1
	105 B	6.33	9.89	2.75	5.28	1.94	0.94	0.45	0.006
High q	Rg (μm)	0.80	0.83	0.78	0.75	0.86	0.79	0.77	0.87
	P	2.10	2.13	2.15	2.03	2.09	2.00	2.08	2.07
	G	0.87	1.15	0.72	0.42	1.30	0.97	1.04	1.61
	108 B	3.25	2.72	2.82	4.01	3.35	6.09	3.14	3.29

Table 1. Guinier radii and exponents as a function of time for acid-treated carbon nanofibers PR19HT.

Bright-field, high-resolution TEM images of the acid-treated nanofibers PR19HT are shown in Figure 2. More defects and even serious damage are found after the acid treatment. Disruption of outer graphitic layers is also observed. The stripping of the altered outer graphite layers after strong oxidation can give rise to thinning of nanofibers. These observations are consistent with the literature. (Shaffer, Fan et al. 1998; Monthioux, Smith et al. 2001)

2.2 Light scattering investigation

There is considerable experimental evidence for the presence of carboxylic acid bound to carbon nanotubes through acid treatment. (Liu, Rinzler et al. 1998; Hu, Bhowmik et al. 2001) These carboxylic groups result in improved dispersion of carbon nanotubes in polar solvents. The carboxylated carbon nanofibers are stable in water for days. In the absence of sonication, however, tubes eventually aggregate and precipitate. We use light scattering to monitor this process.

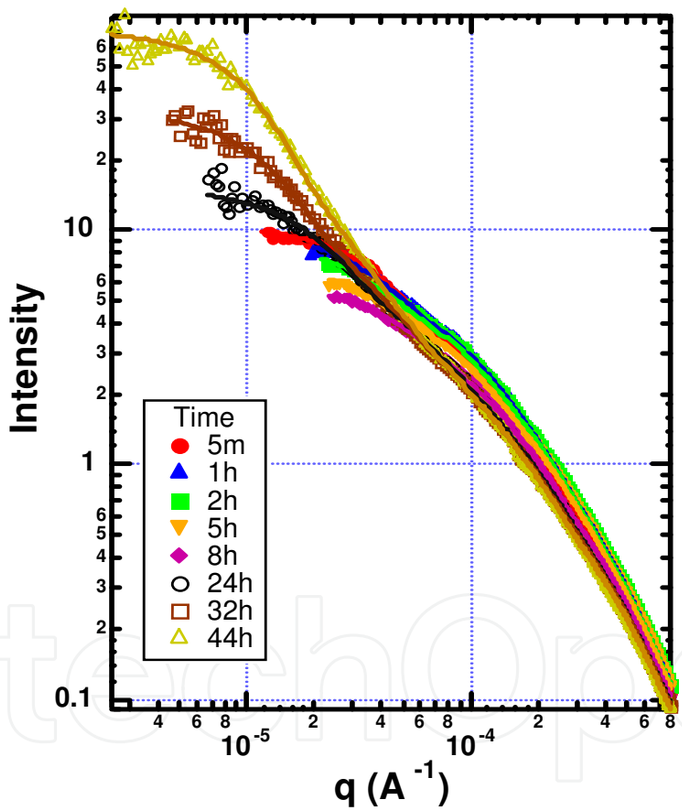


Fig. 3. Dispersion of acid-treated nanofibers PR19HT in water during two-day suspension. The suspensions were sonicated at 10W for five minutes before data were taken using light scattering in batch mode. Minimal change is observed at large q indicating minimal change in morphology below 1 μm. The micron-size entities originally present simply aggregate into larger structures in a hierarchical fashion. The lines are two-level unified fits. The unified parameters are collected in Table 1.

Figure 3 shows the light scattering profiles as a function of time for acid-treated nanofibers PR19HT in water at a concentration of 5.0×10^{-6} g/ml. The data were obtained in the batch

mode with no circulation or sonication. Initially the scattered intensity at low q decreases up to 8 hours. Below we argue that this decrease is due to settling with minimal agglomeration. After 8 h, however, the intensity increases substantially at low-q, consistent with agglomeration. In dilute solution the intensity at q –> 0 is proportional to molecular weight, so the data in Fig. 3 imply an increase of molecular weight by a factor of ten between 8 and 44 hours.

Except for the data near 8 h, two "knees" are observed indicating two length scales. The knee region is referred to as Guinier scattering. The curvature in the Guinier regime defines a length scale (Guinier radius or radius-of-gyration, Rg, in the case of independent scatterers). Each Guinier knee is followed by a quasi power-law regime. The curves were fit using Beaucage's Unified Model to extract Rg, the power-law exponents, P, and the Guinier prefactors, G, and power-law prefactor, B, associated with each length scale. (Beaucage, Schaefer et al. 1994) These parameters are displayed in Table 1 for the two structural levels. The slope near –2 (P = 2) on a log-log plot around q = 0.002 $Å^{-1}$ could arise from a hollow tube since the wall of such an object is a two-dimensional on scales larger than its wall thickness and shorter than the radius. Such a slope, however, can also arise from more complex aggregated structures. (Schaefer, Brown et al. 2003; Schaefer, Zhao et al. 2003) The crossover length scale ($q^{-1} \cong 1$ μm) between the two power-law regimes corresponds to the largest radius of the tube aggregates. Minimal change in Rg and P is observed for $q > 10^{-4}$ $Å^{-1}$, indicating minimal change in morphology with time on length scales below ~1 μm.

The prefactor, G, derived from high-q structural level (level 1) decreases up to 8 hours, indicating that the number and/or molecular weight of the small-scale entities is decreasing up to 8 h. After 8 h, however, the data indicate that these small-scale structure cluster form large-scale objects, which we call agglomerates. All the carbon precipitates after several days. Chen et al observed similar behavior in the region $2 \times 10^{-4} < q < 2 \times 10^{-3}$ for single-walled nanotube suspensions. (Chen, Saltiel et al. 2004)

We also monitored dispersion behavior of untreated carbon nanofibers PR19HT although such a suspension is quite unstable in water even with aid of ultrasound. The data for the untreated sample (Figure 4) show similarities and differences when compared to the treated sample. Although less visible, two structural levels are present and the length scales are similar to the treated case in Figure 3. For the as-received sample, however, the large-scale agglomerates are observed immediately (5 min) whereas they form after 8 h in the treated case. Acid-treatment retards this agglomeration. The overall intensity also shows a nearly monotonic trend with time to lower values consistent with precipitation being the dominant process. The extracted Rgs (Table 2) are virtually unchanged during the precipitation process. The similarity of the length scales for the treated and untreated samples shows that acid treatment does not change the gross morphology of the nanotube aggregates, but only inhibits agglomeration of these smaller scale aggregates. (Zhao, Schaefer et al. 2005)

Figure 5 compares the scattering profile for acid-treated and as-received carbon nanofibers at 5 min after sonication. The intensity at low q (prefactor, G) for the acid-treated sample is one order of magnitude smaller than that for the untreated one, indicating smaller entities in former suspension. Detailed analysis shows that the low-q Guinier radius is 4.8 μm for acid-treated nanofibers, compared to 21.3 μm for untreated nanofibers. These observations are consistent with improved dispersion due to the presence of oxygen-containing functional groups on the surface.

In principle, the morphology of both the small and large-scale objects can be inferred from the power-law exponents, P, since P is the fractal dimension, D, of the objects giving rise to

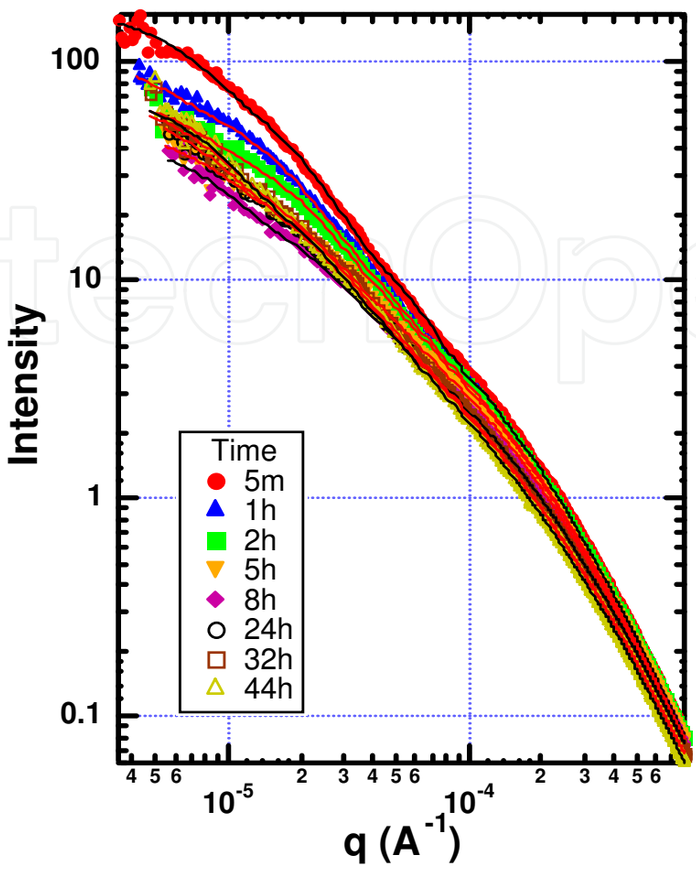


Fig. 4. Evolution of the light scattering profile of un-modified nanofibers PR19HT for two days following dispersion by sonication. The suspensions were sonicated at 10 W for five minutes before the observations began. The measurements were taken in the batch mode, so the sample was undisturbed during the course of the experiment. Note that the intensity at small q is a factor of 10 larger than Fig. 3, implying larger aggregated structures. The lines are two-level unified fits.

	Time	5min	1 hr	2 hr	5 hr	8 hr	24 hr	32hr	44hr
Low q	Rg (μm)	21.3	20.9	20.8	19.4	18.6	19.5	20.1	20.2
	P	1.48	1.44	1.43	1.22	1.23	1.32	1.35	1.40
	G	160.2	110.1	74.2	51.5	44.9	65.2	70.1	74.3
	106 B	0.59	4.23	4.14	29.72	23.24	10.67	8.30	4.43
High q	Rg (μm)	0.86	0.84	0.88	0.83	0.87	0.83	0.83	0.82
	P	2.01	2.07	2.15	2.14	2.08	2.00	1.98	2.10
	G	1.53	1.24	1.46	0.92	1.00	0.67	0.66	0.69
	108 B	4.53	2.93	1.67	1.77	2.56	3.90	4.75	1.89

Table 2. Guinier radii and exponents as a function of time for as-received carbon nanofibers PR19HT.

the scattering. D = 1 implies a linear objects and D > 1 indicates more branched or flexible structures. (Schaefer, Brown et al. 2003; Schaefer, Zhao et al. 2003) For our data, however, the scattering entities are polydisperse and the power-law regions extend over a very limited q range, so this approach is unworkable. An alternative is to use the relationship

$$M_w = R_z^D,$$

where Mw is the weight-average molecular weight, Rz is the weight-squared-average radius and D is the fractal dimension of the object. Since G ~ Mw and Rz ~ Rg, D can be extracted from the slope of a log-log plot of G vs. Rg. Such a plot is shown in Figure 6 for the two structural levels for both the treated and untreated samples. Except for the low-q data for the treated sample, the data imply D ≥ 6, which is unphysical. When the slope is greater than 3 we interpret the evolution of the scattering profile as due to precipitation of carbon, because, to first approximation, G simply decreases at fixed Rg. For the untreated samples, therefore, both structural levels evolve by precipitation.

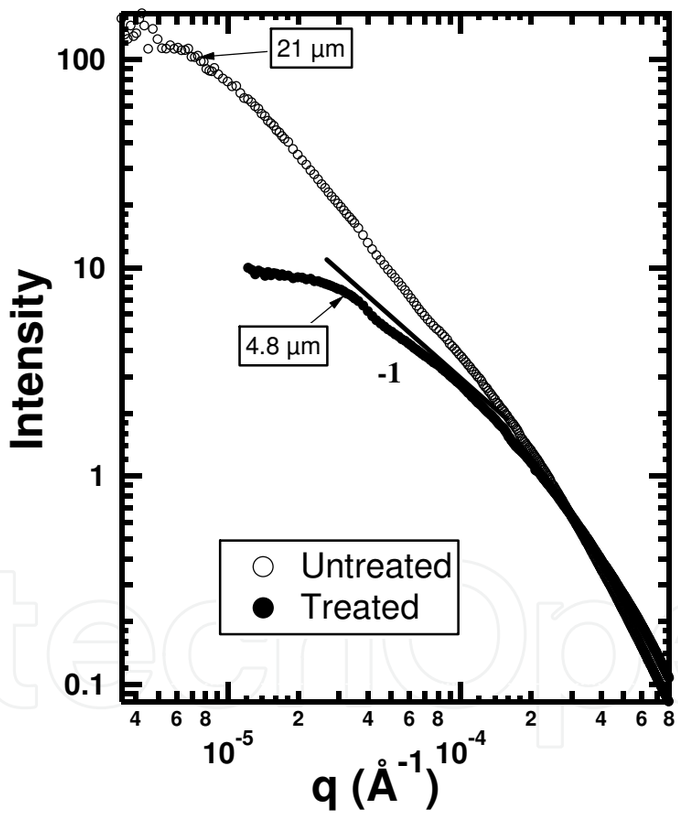


Fig. 5. Comparison of the scattering profiles for untreated and acid-treated carbon nanofibers PR19HT 5 min after sonication. A substantial population large-scale clusters is present only for the untreated sample.

For the treated sample, the small-scale objects precipitate for the first 8 h. and then begin to agglomerate. The latter conclusion is reached because D = 1.7 ± 0.15 for the large-scale structure (Figure 6), consistent with a fractal morphology characteristic of agglomerates formed by kinetic growth. This number is also consistent with the value of P in Table 1 for

the 44-h treated sample. For the other times, the power-law region is insufficient to compare the measured Ps and D from Figure 6. For the treated sample, precipitation dominates agglomeration up to 8 h and agglomeration dominates precipitation after 8 h.

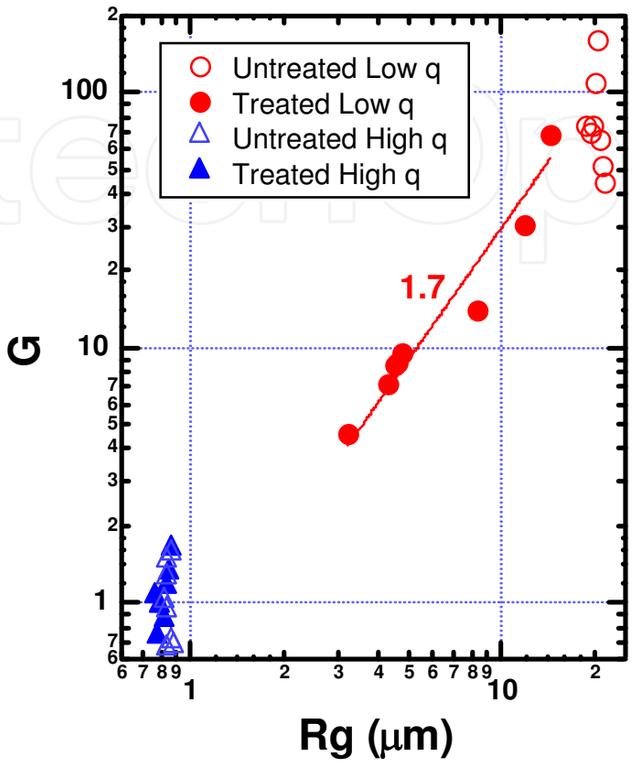


Fig. 6. Relationship between the Guinier prefactors and the Guinier radius for two structural levels observed in Figures 4 and 5. The low-q result for the treated sample is consistent with agglomeration to form a fractal cluster with fractal dimension D = 1.7. In the other cases, the large change in G with minimal change in Rg is consistent with sedimentation.

2.3 Size distribution

In order to further understand the morphology evolution, the data were analyzed to estimate the bundle size distributions using the maximum-entropy method. To extract the size distribution a particle shape must be assumed. Electron microscopy shows that carbon nanofibers are tube-like with some fibers showing more rod-like character. The high-q feature of the data should arise from this one-dimensional morphology.

We investigated both rod and tube models as shown in Figures 7 and 8, which compare the two models for the 8-h acid-treated sample. Figure 5.1.7 shows the fits to the light scattering data. Figure 8 shows the corresponding volume distributions assuming both rod and tube form factors. In the tube case, distributions calculated for different tube-wall thicknesses are shown. For the tube model the fits to the scattering profiles are virtually independent of wall thickness, although the volume distributions show a change in amplitude consistent with the increase of molecular weight with wall thickness, the solid rod being the limiting case. Fortunately, the position and shape of the distribution does not depend strongly on the assumed form factor.

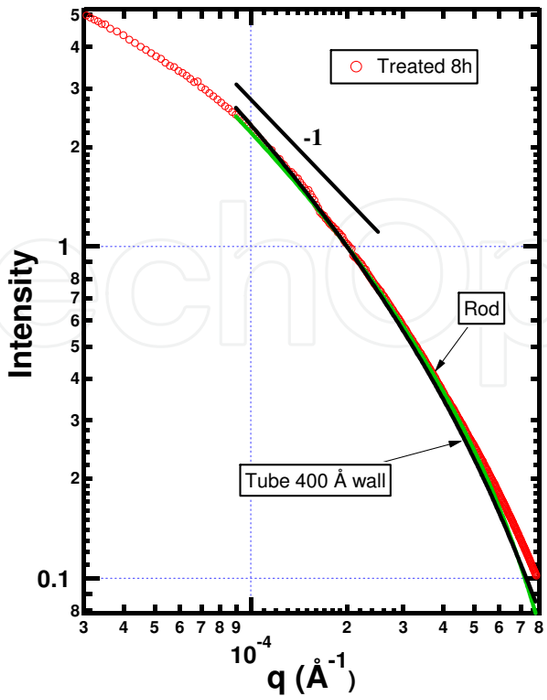


Fig. 7. Maximum-entropy fits to the 8-h treated data assuming rods and tubes. The tube fit is virtually independent of the assumed tube wall thickness. Both rods and tube distributions fit equally well.

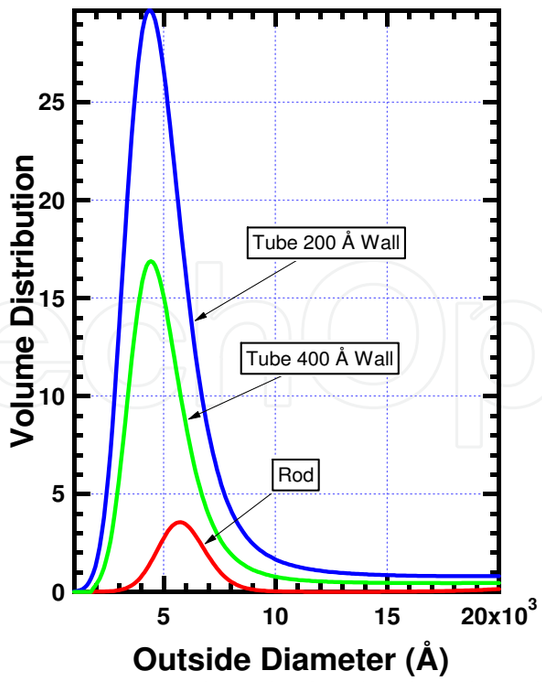


Fig. 8. Volume distributions assuming rods and tubes for the 8-h acid treated data. Both models show diameters somewhat larger than that observed by TEM, indicating some (side-by-side) aggregation.

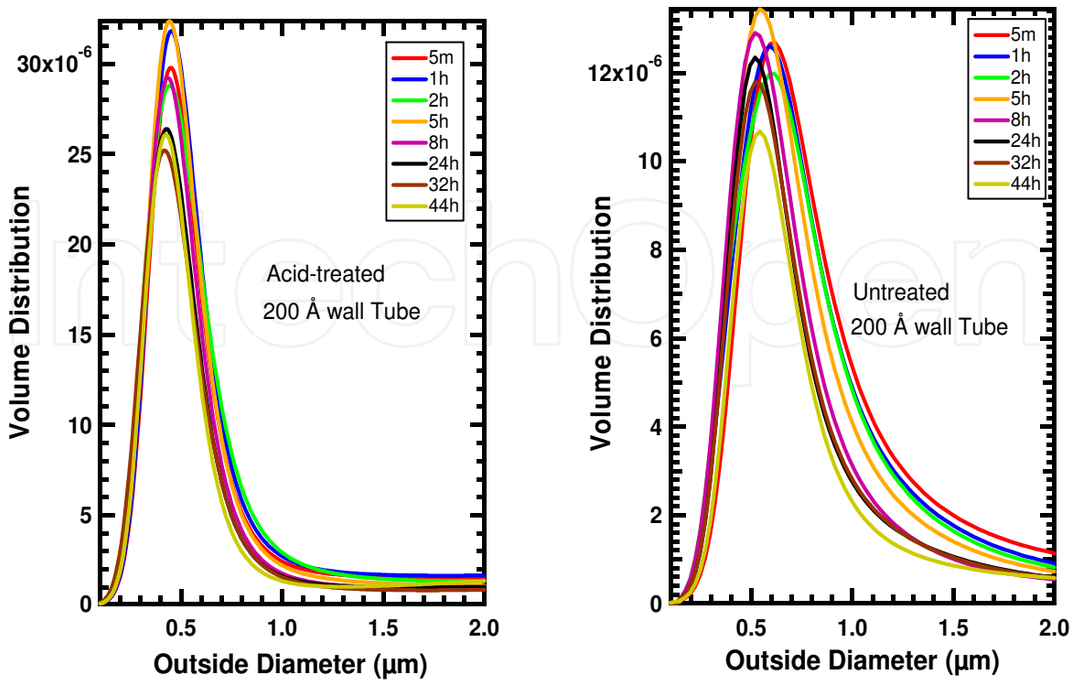


Fig. 9. (a) High-q volume distributions as a function of time for acid-treated nanofibers. The curves are obtained by ME method from light scattering data in the high q region. The particle shape used is tube. The ordinate is arbitrary in that the contrast is not known.
b) High-q volume distributions for untreated nanofibers. The curves are obtained by ME method from light scattering data in the high q region. The particle shape used is tube. Although the ordinate is in arbitrary units, the distributions can be quantitatively compared to Figure 9.

Based on the fits, it is impossible to distinguish between rods and tubes or for that matter more complex structures. Both models give similar results with a peak in the diameter distribution around 0.5 μm. In all cases, the diameter at the peak is considerably larger than the tube diameters seen in TEM. The scattering entities are not individual tubes, but bundles thereof.

Interestingly, the size distributions (Figures 9) extracted from these high-q data show minimal change with time implying that the short-scale morphology is maintained during agglomeration and precipitation. Both the peak position and the tails to larger sizes indicate that dispersion is not complete, based on the tube diameters seen in TEM. The bias to larger sizes is likely due to side-by-side fiber aggregates that are never disrupted. Because light scattering is weighted by volume, it doesn't take much aggregation to produce such tails on the size distributions.

Comparison of Figures 9 (a) and (b) shows that the large-diameter wing of the distribution is suppressed in the acid-treated sample. That is, acid treatment breaks up the larger aggregates. Since the contrast is not known, the volume distributions (ordinate in Figure 9) are on an arbitrary scale. Nevertheless, comparison of the distributions in Figures 9 is meaningful. Based on this comparison, the volume missing from the large-diameter wings

of the treated distributions shows up at around 0.4 μm, which is still substantially larger than the largest individual fibers seen in TEM.

The simplified rod and tube models used here were developed by Justice and Schaefer. (Schaefer, Justice et al. 2005) These models approximate the exact rod and tube models in various power-law regimes and give the proper crossover length scales. Exact models, however, display oscillations in the power-law regimes, which are suppressed in the simplified models. This simplification is of minimal consequence when dealing with polydisperse distributions but it does accelerate the ME fitting code.

Determination of the size distribution for the low-q data is more challenging. In fact, we are not able to extract reasonable size distributions from the low-q portion data using a fractal aggregate model. The process of dispersion and precipitation, however, can be inferred from time evolution of Rg and G extracted from the low-q unified fits. These parameters are found in Table 1.

Figures 10 and 11 show Rg and G derived from low-q region as function of time for acid-treated and untreated nanofibers. For the untreated fibers, G decreases abruptly at constant Rg, consistent with precipitation. After 10 h both Rg and G stabilize. For the treated case, G and Rg increase with time consistent with agglomeration. It is interesting that after 44 h, these parameters approach that of the untreated fibers. These observations are consistent with the fact that acid treatment slows agglomeration and precipitation, but ultimately the fate of the treated fibers is the same as that of the untreated.

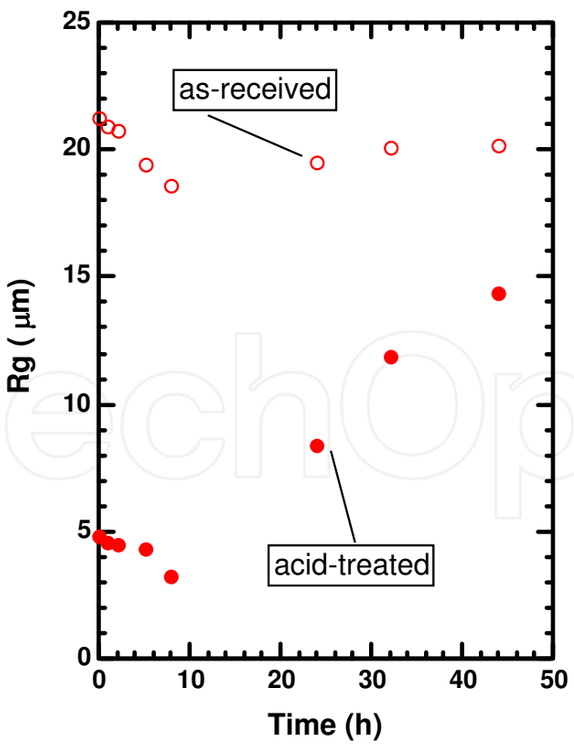


Fig. 10. Rg derived from low q region as a function of time for untreated and acid-treated nanofibers.

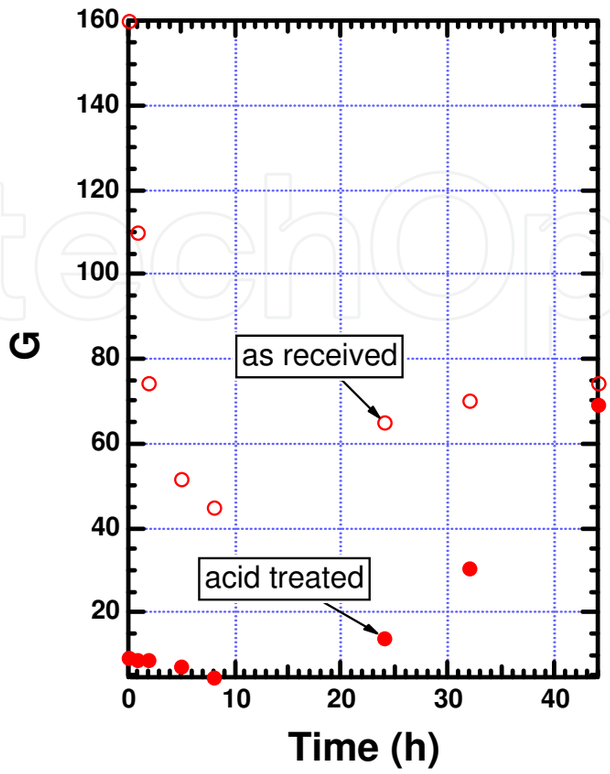


Fig. 11. G derived from low q region as a function of time for untreated and acid-treated nanofibers. At a given concentration G is proportional to the molecular weight.

2.4 Effect of post production processing

In order to optimize their structural features for different applications, these carbon nanofibers are usually processed upon production. Such post production processing can render nanocarbons to possess more desirable strength and electrical conductivity. (http://www.apsci.com/ppi-pyro3.html) For instance, heat treatment (HT) (up to 3000 °C) is performed to graphitize chemical vapor deposited (CVD) carbon present on the surface of as-grown carbon nanofibers. Thus, the heat-treated nanofibers possess highly electrical conductivity. Meanwhile, iron catalysts are removed in this process.

Post production thermal processing also alters surface properties of nanofibers, and thus probably influence their dispersion behavior. The acid-treated nanofibers PR19HT were studied in previous sections. Here we investigate dispersion of another type of acid-treated nanofibers PR19PS. PS means pyrolytically stripped carbon nanofibers. Typically, polyaromatic hydrocarbons are removed during this processing.

Presented in Figure 12, HRTEM images of as-received nanofibers PR19PS show that the naofibers are wrapped with a smooth CVD layer. Defects are occasionally found on the surface. Figure 13 shows typical TEM images of acid-treated PR19PS. Nanofibers with serious damage are observed. The CVD layer becomes rugged and defects are much more obvious along sidewalls after acid treatment.

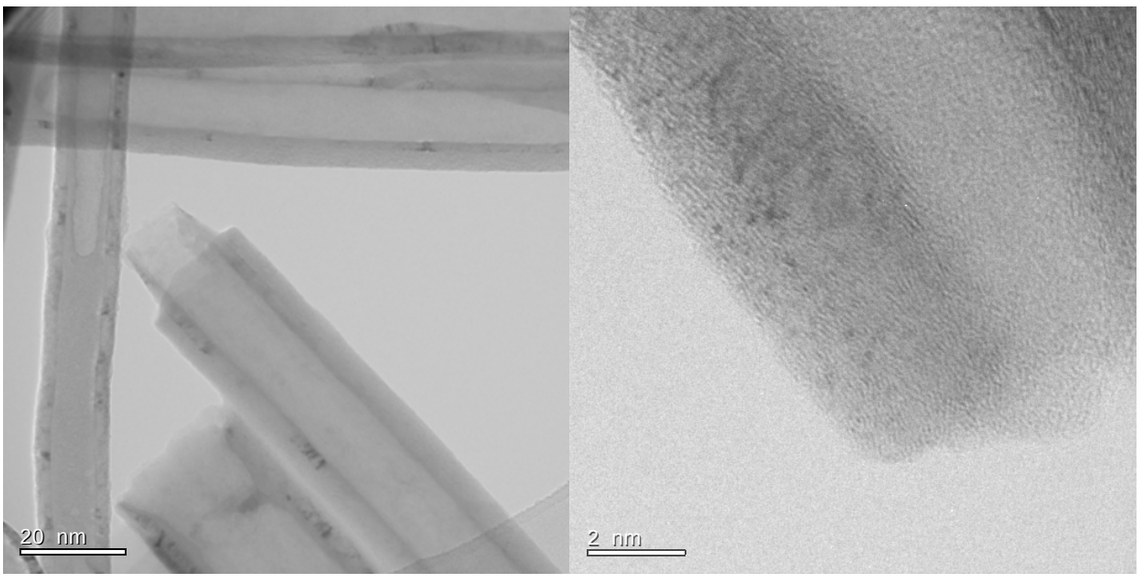


Fig. 12. TEMs of unmodified carbon nanotubes PR19PS. CVD layers are visible at both magnifications. The low-resolution image shows a variety of tube shapes and morphologies including concentric cylinders and stacked cones. The bars are 20 nm and 2 nm.

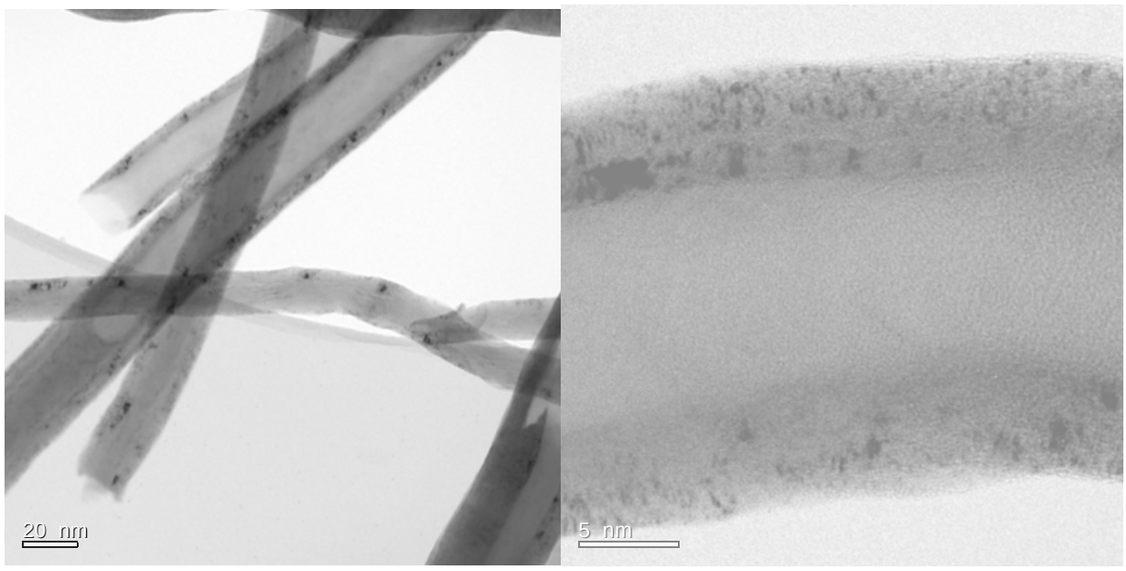


Fig. 13. TEMs of acid-treated PR19PS: More defects on the walls are evident. The bars are 20 nm and 2 nm.

We also measured dispersion behavior of acid-treated nanofibers PR19PS suspended in water using light scattering. Figure 14 shows the light scattering profiles as a function of time for acid-treated nanofibers PR19PS in water at a concentration of 5.0×10^{-6} g/ml. The data were obtained in the batch mode with no circulation or sonication. The overall intensity for acid-treated PR19PS shows similar tendency as acid-treated PR19HT, with an initial decrease followed by substantial increase. The maximal decrease in the intensity at low q is

observed at 21 hr for acid-treated PR19PS whereas it occurs at 8hr for acid-treated PR19HT. That is, acid-treated PR19PS shows slower precipitation process with minimal agglomeration during the initial period. The considerable increase in the intensity at low q indicates agglomeration. Figure 15 compares scattering profiles of acid-treated PR19HT at 44 hr and PR19PS at 120 hr. Minimal difference in intensity at low q for both cases implies slower agglomeration for acid-treated PR19PS.

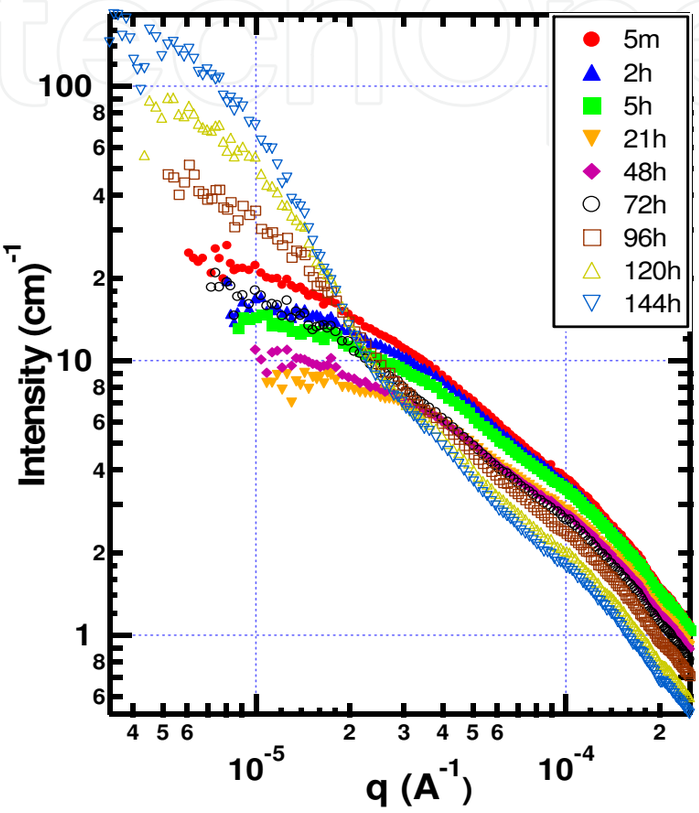


Fig. 14. Dispersion of acid-treated nanofibers (PR19PS) in water during four-day suspension. The suspensions were sonicated at 10W for five minutes before data were taken using light scattering in batch mode.

The scattering curves consist of one quasi power-law regimes and one Guinier regime. The curves were fit using Beaucage's Unified Model to extract Rg, the power-law exponents, P, and the Guinier prefactors, G, and power-law prefactor, B.(Beaucage, Schaefer et al. 1994) These parameters are listed in Table 3.

Figures 16 and 17 show Rg and G as a function of time for acid-treated nanofibers PR19PS and PR19HT. Following initial decrease due to precipitation, Rgs for acid-treated PR19PS nanofibers show a gradual increase over time whereas Rg for acid-treated PR19HT increase dramatically. It takes 120 hr for treated PR19PS to approach the Rg at 44 hr for treated PR19HT. At this Rg (≅ 15 μm), G derived from treated PR19PS is much larger than that from treated PR19HT, indicating that more carbon entities are present in treated PR19PS suspension. Acid-treated PR19PS is suspended longer in water and agglomerates slowly.

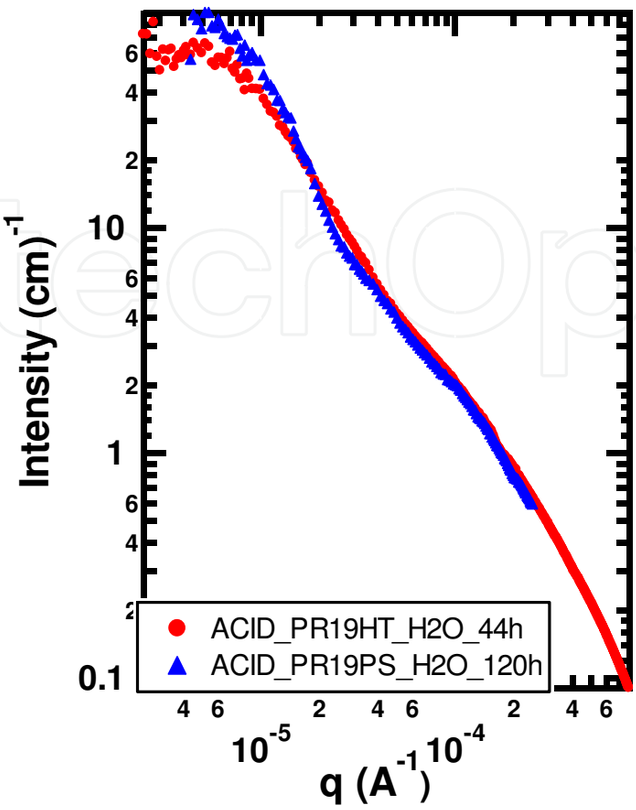


Fig. 15. Comparison of the scattering profiles for acid-treated carbon nanofibers PR19HT and PR19PS.

Time	5min	2 hr	5 hr	21 hr	48 hr	72 hr	96 hr	120 hr	144 hr
Rg (μm)	7.4	4.9	4.5	3.5	4.4	7.6	12.4	15.9	16.6
P	1.18	1.25	1.26	1.35	1.24	1.13	1.11	1.15	1.18
G	23.34	16.47	14.06	9.03	10.61	18.52	48.42	97.81	158.92
105 B	6.67	3.54	3.04	1.25	3.28	7.66	7.64	4.70	2.95

Table 3. Guinier radii and exponents as a function of time for acid-treated carbon nanofibers PR19PS.

Due to their graphete nature, the sidewalls of nanofibers PR19HT possess a chemical stability. However, the presence of CVD layers on the surface of PR19PS makes the chemistry available for surface modification less restrictive. Thus, PR19PS is more vulnerable to oxidative attack. Acid treatment creates denser surface acid sites that slow precipitation and agglomeration.

3. PEG-functionalized nanofibers

The presence of oxygen-containing groups on nanofibers after acid treatment provides rich chemistry for the attachment of functional groups to the surface of nanofibers. The simplest

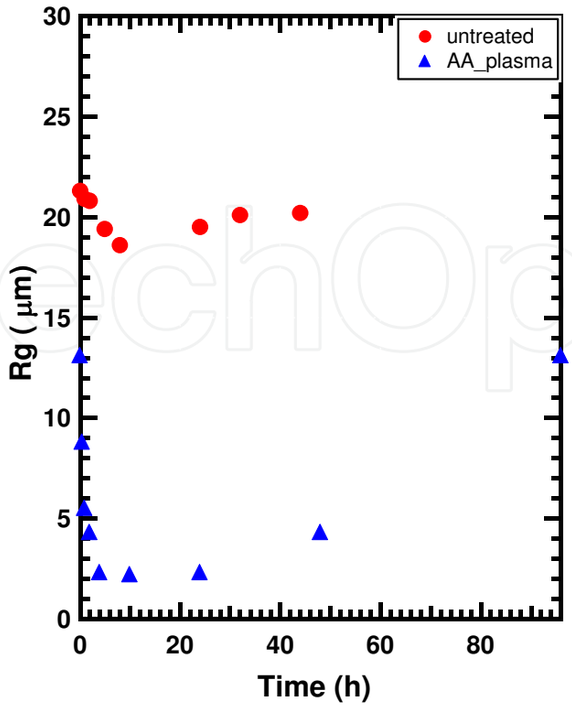


Fig. 16. Rg derived from low q region as a function of time for acid-treated nanofibers PR19PS and PR19HT.

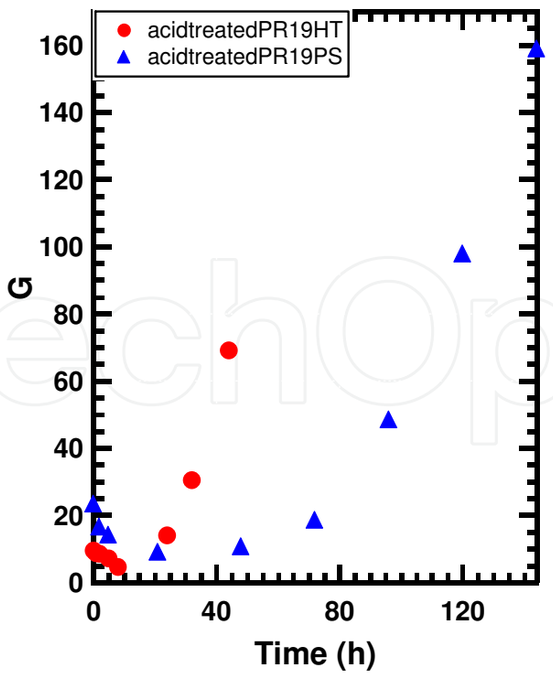


Fig. 17. G derived from low q region as a function of time for acid-treated nanofibers PR19PS and PR19HT. At a given concentration G is proportional to the molecular weight.

route to the dissolution of the nanofibers is to directly react an amine with the carboxylated nanofibers. A zwiterion is produced through a simple acid-base reaction. (Huang, Fernando et al. 2003)

Through the acid-base zwitterion interaction, diamine-terminated oligomeric poly(ethylene glycol) (PEG) was reacted with the carboxylic acids, which are bound to nanofibers via acid treatment. This process yields a dark-colored homogeneous solution that is stable in water for months. The dispersion was characterized using light scattering.

Figure 18 shows the light scattering profiles as a function of time for PEG-functionalized nanofibers (PR19HT) in water at a concentration of 5.0 × 10-6 g/ml. The data were obtained in the batch mode with no circulation or sonication. The scattering curve does not change with time. No Rg (radius of gyration) can be extracted in limiting regime due to the absence of a crossover at low q. The slope near –1 in this regime indicates a rod-like character on large scales. The slope near –2 (P = 2) on a log-log plot around q = 0.003 Å -1 may arise from a hollow tube.

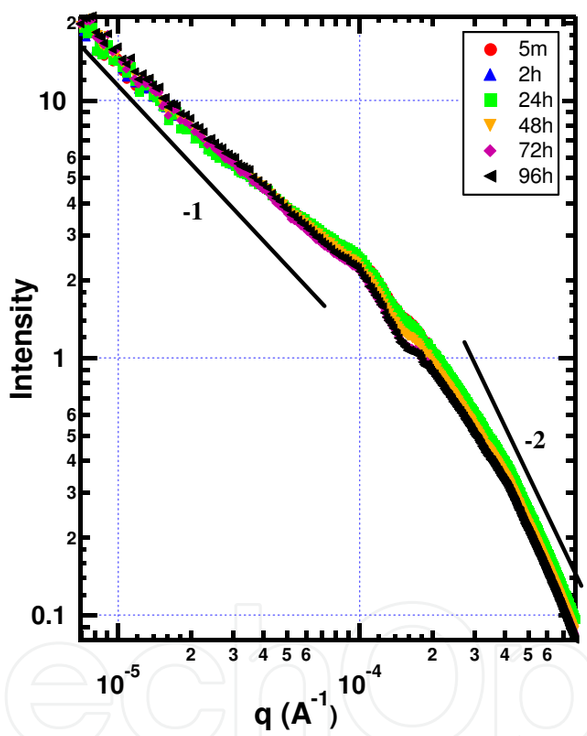


Fig. 18. Evolution of the light scattering profile of PEG-functionalized nanofibers (PR19HT) for four days following dispersion by sonication. The suspensions were sonicated at 10 W for five minutes before the observations began. The measurements were taken in the batch mode, so the sample was undisturbed during the course of the experiment.

Figure 19 compares the scattering profiles for PEG-functionlized, acid-treated and as-purchased carbon nanofibers at 44h after sonication. Compared to PEG-functionalized sample, Guinier region at low q is observed for untreated and acid-treated nanofibers, indicating the presence of large-length-scale structures formed by the small-scale structures at high q. In untreated state, as described above, the suspension is quite unstable and fibers precipitate. The large-scale objects we call agglomerates are observed immediately after

sonication. The Guinier prefactors G derived from low-q region using Beaucage's Unified Model decrease abruptly right after sonication at fixed Rg, consistent with precipitation being dominant process. Such agglomeration is observed after 24 h for acid-treated case. After 44 h, the scattering curve of acid-treated sample approaches that of untreated fibers. The presence of oxygen-containing groups on the surface of nanofibers through acid treatment can not stop agglomeration and precipitation, but retard these processes.

Solubility is a measure of an equilibrium between the dissolved phase and aggregated (or agglomerated) phase. A long solubilizing chain on the functionalities should be favorable to obtain soluble nanofibers. Compared to the acid-treated and untreated sample, which shows strong agglomeration and no rod-like behavior, PEG-functionalized nanofibers do not show any agglomeration over time. Attachment of water-soluble oligemeric PEG on nanofibers does shift the equilibrium towards the dissolved phase, preventing agglomeration. (Zhao & Schaefer 2008)

In order to further understand the effect of the functionalization on the morphology, the data were analyzed by fitting with a simplified tube or rod form factor. The crossover length scale at high q between the two power-law regimes corresponds to the largest radius of the individual fibers or fiber aggregates. We argue below that the scattering objects are side-by-side fiber aggregates or bundles.

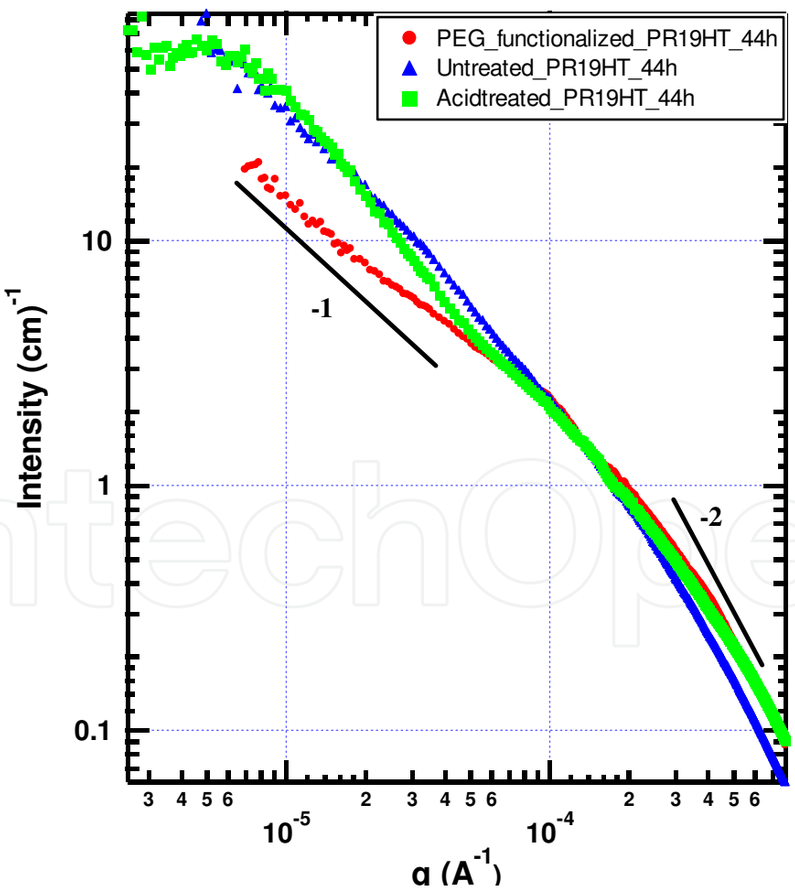


Fig. 19. Comparison of the scattering profiles for PEG-functionalized, untreated and acid-treated carbon nanofibers 44 hr after sonication.

The data do not fit with a rod form factor although they do follow a tube-like form factor reasonably well. We fit the scattering curve of PEG-functionalized nanofibers at 72 h using a simplified tube form factor (Figure 20). The simplified tube form factor approximates an exact tube model but suppress the oscillations that are found for exact models.(Justice, Wang et al. 2007) The simplified tube model fits the data reasonably well except at intermediate q, where it seems to underestimate the size of the relevant size scale (tube outer radius).

Based on the fit to the simplified tube form factor, one might naively conclude that dispersion is down to the level of individual tubes. However, the outer diameter of 0.47 μm (calculated from the radius of 2350 Å) derived from the simplified tube model is substantially larger than the largest individual fibers seen in TEM. That is, scattering entities are not individual tubes, but side-by-side fiber bundles. A bundled structure also accounts for the deviation from the simplified tube form factor. Nevertheless, fitting with the simplified tube model implies that these fiber aggregates are rigid and isolated. Time-evolution of dispersion behavior of PEG-nanofibers shows that fiber bundles remain well dispersed and do not form large-scale agglomerates over weeks.

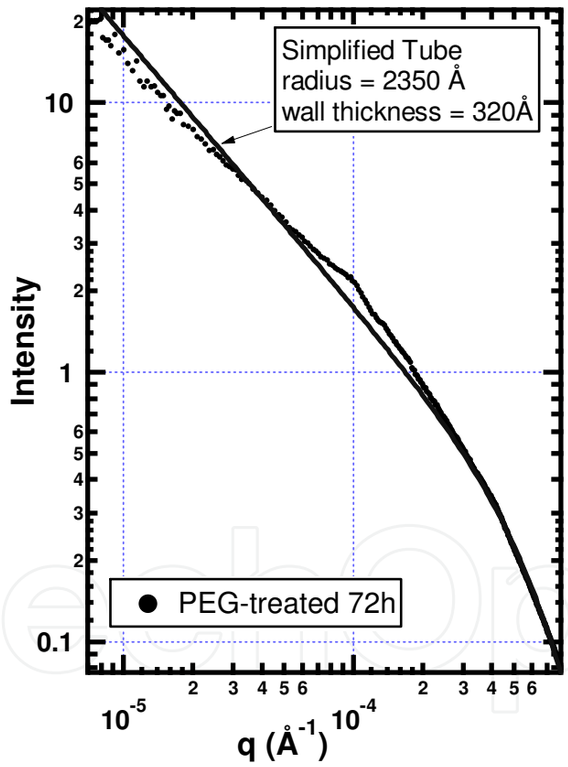


Fig. 20. Light scattering data for PEG-functionalized nanofibers compared with the simplified tube model.

4. Plasma-treated nanofibers

Plasma polymerization has been an active area of research over the past decades. (van Ooij, Zhang et al. 1999) This technique has been used in surface and interface engineering for improving adhesion, hydrophobicity and hydrophilicity, corrosion resistance or for surface

etching. Low temperature plasma polymerization, a room temperature and environmentally benign process, can be used for surface modification and thin film deposition on almost all substances. Deposition of ultrathin films on nanoparticles by plasma treatment has been achieved. (Shi, Lian et al. 2002; Shi, Lian et al. 2003)

To enhance dispersion ability of carbon nanofibers in water, acrylic acid is selected as a monomer for plasma polymerization. (Shi, He et al. 2002)Bright-field and high-resolution TEM images of the plasma-coated nanofibers are shown in Figure 21. An ultrathin film amorphous layer can be clearly seen covering the surface of the carbon nanofibers. The thin film is uniform with a thickness of approximately 2-7 nm surrounding the entire nanofiber surface. In our experiment, carbon nanofibers are treated by plasma polymerization. Brief plasma treatment deposits a coating of highly crosslinked polymer on the fibers, which substantially improves their compatibility with water, and thus assists dispersion of carbon nanofibers.

We measured dispersion efficiency of AA-plasma-treated nanofibers suspended in water and made a comparison with untreated nanofibers. Figure 22 shows the light scattering profiles as a function of time for acrylic acid (AA) plasma-treated nanofibers PR19HT in water at a concentration of 5.0 × 10-6 g/ml. The data were obtained in the batch mode with no circulation or sonication. For untreated nanofibers, as described above, the overall intensity shows a nearly monotonic, gradual decrease consistent with precipitation being the dominant process. After plasma treatment, the intensity at low q tends to drop abruptly with time. At 10 hr, the maximal decrease in the intensity is observed. After 10 hr, however, the intensity increases substantially, consistent with agglomeration.

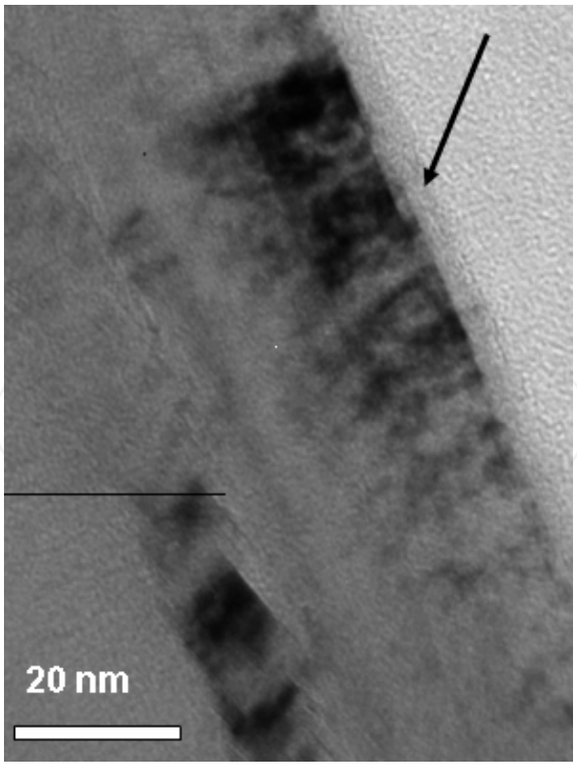


Fig. 21. TEM image of plasma-treated carbon nanofibers PR19LHT: The bars are 10 nm. An ultrathin film of acrylic acid was observed on the surface of the nanofibers.

	Time	5min	30min	1hr	2 hr	4hr	8hr	24hr	48 hr	96 hr
Low q	Rg (μm)	13.1	8.8	5.5	4.3	2.3	2.2	2.3	4.3	13.1
	P	1.58	1.43	1.39	1.22	1.21	1.20	1.20	1.47	1.70
	G	70.78	31.13	14.52	7.68	3.48	1.92	2.90	10.35	36.40
	106 B	70.31	3.26	4.41	21.87	13.81	10.84	15.50	1.47	17.06
High q	Rg (μm)	0.67	0.72	0.71	0.65	0.71	0.73	0.68	0.69	0.67
	P	1.93	2.07	1.90	1.97	1.97	1.90	1.95	1.94	2.10
	G	0.73	0.55	0.58	0.37	0.48	0.58	0.42	0.43	0.32
	108 B	6.58	1.14	11.34	5.69	5.67	29.6	5.55	4.92	1.64

Table 4. Guinier radii and exponents as a function of time for plasma-treated carbon nanofibers.

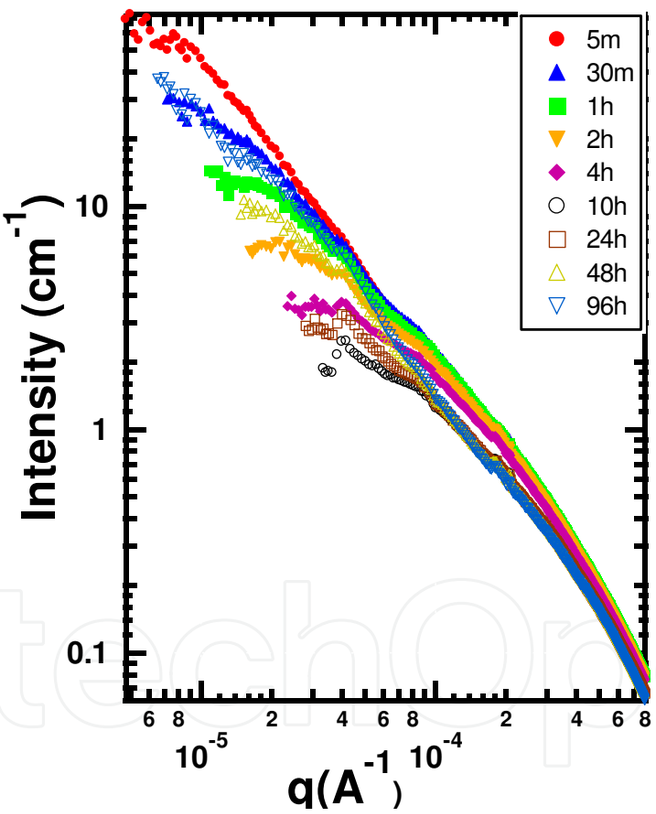


Fig. 22. Evolution of the light scattering profile of plasma-treated nanofibers in water for four days following dispersion by sonication. The suspensions were sonicated at 10W for five minutes before the observations began. The measurements were taken in the batch mode.

The scattering curves consist of two power-law regimes and two Guinier regimes that define two "length scales". Each Guinier regime is followed by a quasi power-law regime. The curves were fit using Beaucage's Unified Model to extract Rg, the power-law exponents, P, and the Guinier prefactors, G, and power-law prefactor, B, associated with each length scale.

These parameters are displayed in Table 4 for the two structural levels. The high q data share similarity with that for the untreated sample. These data imply minimal change in morphology with time on length scales below ~1 μm.
The decrease in the scattered intensity at low q up to 10 hours is pronounced and ascribed to precipitation. After 10 hr, however, the large-scale agglomerates gradually form.
Figure 23 compares the scattering profile for plasma-treated and as-purchased carbon nanofibers PR19HT at 10 hr after sonication. Compared to the untreated sample, the intensity at low q (G) for the treated sample is much smaller, indicating small entities in the suspension. The extracted length scale Rg at 10 hr, 2.2 μm is consistent with much smaller agglomerates compared to the untreated case. After 10 hours there is evidence for agglomeration. Plasma treatment retards this agglomeration.
Figures 24 and 25 show Rg and G derived from low-q region as a function of time for plasma-treated and untreated nanofibers. In both cases, G decreases during the first ten hours, consistent with precipitation. After 10 h, G increases with time consistent with agglomeration (increased Rg) for the plasma-treated sample, whereas both Rg and G show minor change for the untreated sample. Rgs extracted from the plasma-treated sample is considerably smaller than those in the untreated case, indicating improved dispersion.
After plasma treatment, the carbon stays suspended much longer although all the fibers precipitate finally. The clusters are much easier to break up and more difficult to agglomerate. Plasma treatment improves compatibility with water, thus slowing agglomeration and precipitation.

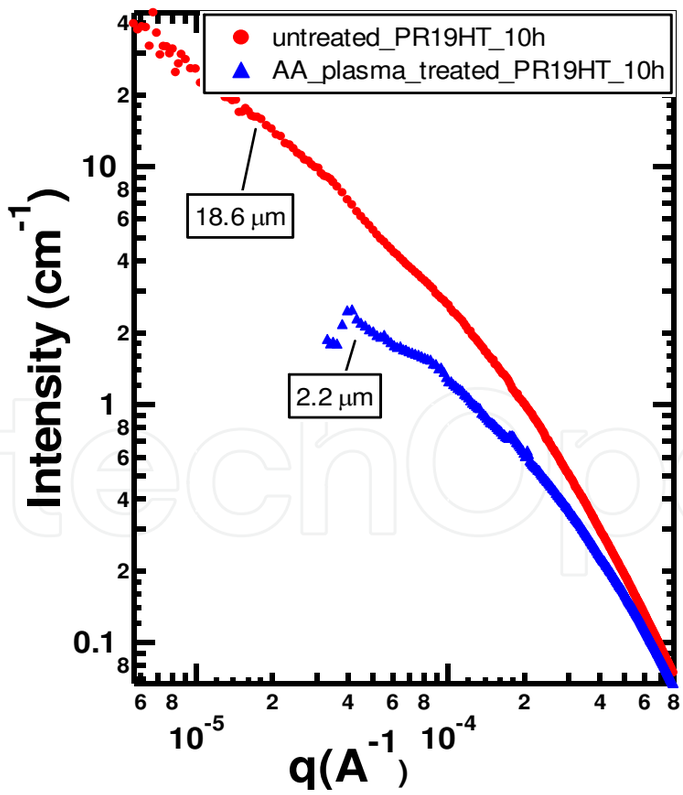


Fig. 23. Comparison of the scattering profiles for untreated and plasma-treated carbon nanofibers 8 h after sonication. A substantial population of large-scale clusters is present only for the untreated sample.

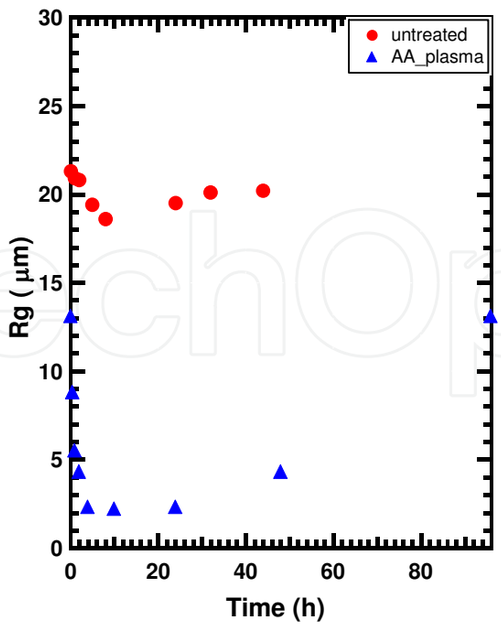


Fig. 24. Rg derived from low q region as a function of time for untreated and plasma-treated nanofibers.

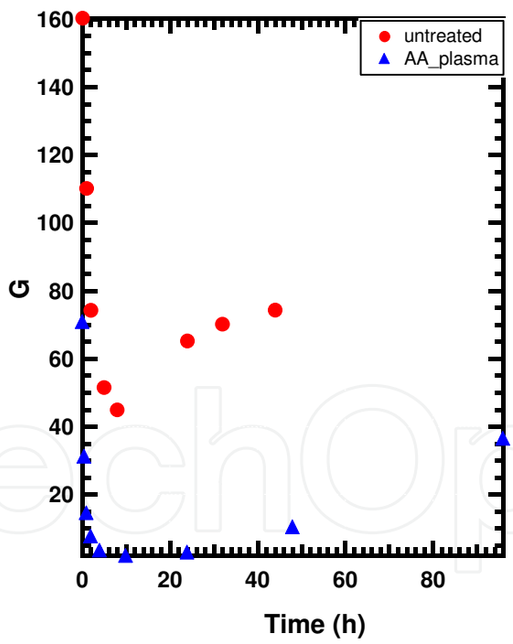


Fig. 25. G derived from low q as a function of time for untreated and plasma-treated nanofibers. At a given concentration region G is proportional to the molecular weight.

5. Summary

Dispersion of nanotubes in suspensions has been investigated using light scattering. Functionalization, plasma treatment and surfactants were used to assist dispersion. Improved dispersion in solutions was achieved. The main conclusions are summarized as follows.

We compare dispersion behavior of acid-treated and as-received carbon nanofibers suspended in water under quiescent conditions. Both samples show a hierarchical morphology consisting small-scale aggregates and large-scale agglomerates. The aggregates could be side-by-side bundles of individual nanofibers or more complex structures. In any case these objects agglomerate to form large-scale fractal clusters. Acid treatment shifts the small-scale size distributions to smaller bundle sizes. In the absence of surface treatment these bundles agglomerate immediately after sonication. In the acid-treated case, by contrast, it takes many hours for the agglomerates to form. Thus acid treatment assists dispersion primarily by retarding large-scale agglomeration not by suppressing small-scale aggregation. Post production processing affects dispersion. Acid-treated PR19PS shows slower agglomeration and precipitation than acid-treated PR19HT.

Dispersion behavior of PEG-functionalied nanofibers suspended in water in a quiescent condition was investigated. Comparison with untreated and acid-treated carbon nanofibers show that PEG-functionalization completely prevents formation of large-scale agglomerates that consist of small scale side-by-side aggregates. The presence of PEG oligomer has little effect on the small-scale bundle size distributions. Prevention of agglomeration is the primary mechanism by which functionalization leads to solubilization of nanofibers.

Nanofibers are plasma-treated using acrylic acid as a monomer. The plasma-treated nanofibers show greater tendency to suspend. The presence of COOH on the nanofibers could alter the surfaces of carbon nanofibers towards hydrophilicity, thus improving dispersion of nanofibers in water.

6. References

Ausman, K. D., R. Piner, et al. (2000). "Organic solvent dispersions of single-walled carbon nanotubes: Toward solutions of pristine nanotubes." Journal of Physical Chemistry B 104(38): 8911-8915.

Beaucage, G., D. W. Schaefer, et al. (1994). "Multiple Size Scale Structures in Silica Siloxane Composites Studied by Small-Angle Scattering." Abstracts of Papers of the American Chemical Society 207: 144-149.

Bechinger, C., D. Rudhardt, et al. (1999). "Understanding depletion forces beyond entropy." Physical Review Letters 83(19): 3960-3963.

Boukari, H., G. G. Long, et al. (2000). "Polydispersity during the formation and growth of the Stober silica particles from small-angle X-ray scattering measurements." Journal of Colloid and Interface Science 229(1): 129-139.

Chen, J., M. A. Hamon, et al. (1998). "Solution properties of single-walled carbon nanotubes." Science 282(5386): 95-98.

Chen, J., A. M. Rao, et al. (2001). "Dissolution of full-length single-walled carbon nanotubes." Journal of Physical Chemistry B 105(13): 2525-2528.

Chen, Q., C. Saltiel, et al. (2004). "Aggregation behavior of single-walled carbon nanotubes in dilute aqueous suspension." Journal of Colloid and Interface Science 280: 91-97.

Dresselhaus, M. S., G. Dresselhaus, et al. (2001). Carbon Nanotubes: Synthesis, Structure, Properties and Applications. Berlin, Springer.

Gong, Q., Z. Li, et al. (2005). "Synthesis and characterization of in situ grown carbon nanofiber/nanotube reinforced carbon/carbon composites." Carbon 43: 2426-2429.

Hu, H., P. Bhowmik, et al. (2001). "Determination of the acidic sites of purified single-walled carbon nanotubes by acid-base titration." Chemical Physics Letters 345(1-2): 25-28.

Huang, W. J., S. Fernando, et al. (2003). "Solubilization of single-walled carbon nanotubes with diamine-terminated oligomeric poly(ethylene glycol) in different functionalization reactions" Nano letters 3(4): 565-568.
Ilavsky, J. (2004). Particle Size ditribution from USAX, Irena SAS Modeling Macros Manual, UNICAT,Argonne Illinois, USA.
Jemian, P. R., J. R. Weertman, et al. (1991). "Characterization of 9cr-1movnb Steel by Anomalous Small-Angle X-Ray-Scattering." Acta Metallurgica Et Materialia 39(11): 2477-2487.
Justice, R. S., D. H. Wang, et al. (2007). "Simplified tube form factor for analysis of small-angle scattering data from carbon nanotube filled systems." Journal of Applied Crystallography 40: S88-S92.
Li, P., T. Zhao, et al. (2005). "Deuterated water as super solvent for short carbon nanotubes wrapped by DNA." Carbon 43: 2701-2703.
Liu, J., A. G. Rinzler, et al. (1998). "Fullerene pipes." Science 280(5367): 1253-1256.
Monthioux, M., B. W. Smith, et al. (2001). "Sensitivity of single-wall carbon nanotubes to chemical processing: an electron microscopy investigation." Carbon 39(8): 1251-1272.
Morrison, J. D., J. D. Corcoran, et al. (1992). "The Determination of Particle-Size Distributions in Small-Angle Scattering Using the Maximum-Entropy Method." Journal of Applied Crystallography 25: 504-513.
Potton, J. A., G. J. Daniell, et al. (1988). "Particle-Size Distributions from Sans Data Using the Maximum- Entropy Method." Journal of Applied Crystallography 21: 663-668.
Safadi, B., R. Andrews, et al. (2002). "Multiwalled carbon nanotube polymer composites: synthesis and characterization of thin films " J. Appl. Poly. Sci. 84: 2660-2669.
Schaefer, D. W. (1988). "Fractal models and the structure of materials." Materials Research Society Bulletin 13(2): 22.
Schaefer, D. W., J. M. Brown, et al. (2003). "Structure and dispersion of carbon nanotubes." Journal of Applied Crystallography 36: 553-557.
Schaefer, D. W., B. C. Bunker, et al. (1989). "Fractals and Phase-Separation." Proceedings of the Royal Society of London Series a- Mathematical Physical and Engineering Sciences 423(1864): 35-53.
Schaefer, D. W., R. S. Justice, et al. (2005). "Large-Scale Morphology of Dispersed Layered Silicates " Materials Research Society symposia proceedings 840: Q3.3.1-3.3.6.
Schaefer, D. W., J. Zhao, et al. (2003). "Morphology of Dispersed Carbon Single-Walled Nanotubes." Chemical Physics Letters 375(3-4): 369-375.
Shaffer, M. S. P., X. Fan, et al. (1998). "Dispersion and packing of carbon nanotubes." Carbon 36(11): 1603-1612.
Shi, D. L., P. He, et al. (2002). "Plasma deposition and characterization of acrylic acid thin film on ZnO nanoparticles." Journal of Materials Research 17(10): 2555-2560.
Shi, D. L., J. Lian, et al. (2002). "Plasma deposition of Ultrathin polymer films on carbon nanotubes." Applied Physics Letters 81(27): 5216-5218.
Shi, D. L., J. Lian, et al. (2003). "Plasma coating of carbon nanofibers for enhanced dispersion and interfacial bonding in polymer composites." Applied Physics Letters 83(25): 5301-5303.
van Ooij, W. J., N. Zhang, et al. (1999). Fundamental and Applied Aspects of Chemically Modified Surfaces, Royal Society of Chemistry.
Zhao, J. and D. W. Schaefer (2008). "Morphology of PEG-Functionalized Carbon Nanofibers in Water." Journal of Physical Chemistry C 112: 15306 - 15310.
Zhao, J., D. W. Schaefer, et al. (2005). "How Does Surface Modification Aid in the Dispersion of Carbon Nanofibers?" Journal of Physical Chemistry B 109: 23351-23357.



Nanofibers

Edited by Ashok Kumar

ISBN 978-953-7619-86-2
Hard cover, 438 pages
Publisher InTech
Published online 01, February, 2010
Published in print edition February, 2010

“There’s Plenty of Room at the Bottom” this was the title of the lecture Prof. Richard Feynman delivered at California Institute of Technology on December 29, 1959 at the American Physical Society meeting. He considered the possibility to manipulate matter on an atomic scale. Indeed, the design and controllable synthesis of nanomaterials have attracted much attention because of their distinctive geometries and novel physical and chemical properties. For the last two decades nano-scaled materials in the form of nanofibers, nanoparticles, nanotubes, nanoclays, nanorods, nanodisks, nanoribbons, nanowhiskers etc. have been investigated with increased interest due to their enormous advantages, such as large surface area and active surface sites. Among all nanostructures, nanofibers have attracted tremendous interest in nanotechnology and biomedical engineering owing to the ease of controllable production processes, low pore size and superior mechanical properties for a range of applications in diverse areas such as catalysis, sensors, medicine, pharmacy, drug delivery, tissue engineering, filtration, textile, adhesive, aerospace, capacitors, transistors, battery separators, energy storage, fuel cells, information technology, photonic structures and flat panel displays, just to mention a few. Nanofibers are continuous filaments of generally less than about 1000 nm diameters. Nanofibers of a variety of cellulose and non-cellulose based materials can be produced by a variety of techniques such as phase separation, self assembly, drawing, melt fibrillation, template synthesis, electro-spinning, and solution spinning. They reduce the handling problems mostly associated with the nanoparticles. Nanoparticles can agglomerate and form clusters, whereas nanofibers form a mesh that stays intact even after regeneration. The present book is a result of contributions of experts from international scientific community working in different areas and types of nanofibers. The book thoroughly covers latest topics on different varieties of nanofibers. It provides an up-to-date insightful coverage to the synthesis, characterization, functional properties and potential device applications of nanofibers in specialized areas. We hope that this book will prove to be timely and thought provoking and will serve as a valuable reference for researchers working in different areas of nanofibers. Special thanks goes to the authors for their valuable contributions.

How to reference

In order to correctly reference this scholarly work, feel free to copy and paste the following:

Jian Zhao (2010). Morphology and Dispersion of Pristine and Modified Carbon Nanofibers in Water, Nanofibers, Ashok Kumar (Ed.), ISBN: 978-953-7619-86-2, InTech, Available from: http://www.intechopen.com/books/nanofibers/morphology-and-dispersion-of-pristine-and-modified-carbon-nanofibers-in-water

INTECH
open science | open minds

InTech Europe
University Campus STeP Ri
Slavka Krautzeka 83/A
51000 Rijeka, Croatia
Phone: +385 (51) 770 447
Fax: +385 (51) 686 166
www.intechopen.com

InTech China
Unit 405, Office Block, Hotel Equatorial Shanghai
No.65, Yan An Road (West), Shanghai, 200040, China
中国上海市延安西路65号上海国际贵都大饭店办公楼405单元
Phone: +86-21-62489820
Fax: +86-21-62489821

IntechOpen

IntechOpen

© 2010 The Author(s). Licensee IntechOpen. This chapter is distributed under the terms of the Creative Commons Attribution-NonCommercial-ShareAlike-3.0 License, which permits use, distribution and reproduction for non-commercial purposes, provided the original is properly cited and derivative works building on this content are distributed under the same license.

IntechOpen

IntechOpen